

S4Sleep: Elucidating the design space of deep-learning-based sleep stage classification models

Tiezhi Wang^a, Nils Strodthoff^{a,*}

^a*Carl von Ossietzky Universität Oldenburg, Ammerlaender Heerstr.
114-118, Oldenburg, 26129, Lower Saxony, Germany*

Abstract

Scoring sleep stages in polysomnography recordings is a time-consuming task plagued by significant inter-rater variability. Therefore, it stands to benefit from the application of machine learning algorithms. While many algorithms have been proposed for this purpose, certain critical architectural decisions have not received systematic exploration. In this study, we meticulously investigate these design choices within the broad category of encoder-predictor architectures. We identify robust architectures applicable to both time series and spectrogram input representations. These architectures incorporate structured state space models as integral components and achieve statistically significant performance improvements compared to state-of-the-art approaches on the extensive Sleep Heart Health Study dataset. We anticipate that the architectural insights gained from this study along with the refined methodology for architecture search demonstrated herein will not only prove valuable for future research in sleep staging but also hold relevance for other time series annotation tasks.

Keywords: Decision support systems, Electroencephalography, Machine learning algorithms, Time series analysis

*corresponding author: nils.strodthoff@uol.de

1. Introduction

Sleep disorders, which are prevalent and can have severe implications for patients' health and overall well-being, are known to lead to significant morbidity [1, 2]. Primary care practice commonly involves managing various significant sleep disorders including insomnia, sleep-disordered breathing, hypersomnia/narcolepsy, circadian rhythm disorders, parasomnias, and sleep-related movement disorders [2]. Within clinical practice, sleep staging is necessary to understand the structure and quality of sleep, enabling the diagnosis of sleep disorders and informing appropriate treatment strategies. It also facilitates sleep research, providing insights into sleep patterns and physiological processes during different stages of sleep.

Sleep staging: Sleep staging refers to inferring the state of human sleep into one of five or six sleep stages: wake stage (W), non-rapid-eye-movement (NREM) stages (N1-N3 or N1-N4 depending on the annotation standard), rapid-eye-movement stage (REM). The gold standard measurement setup for sleep staging is polysomnography (PSG), which typically comprises a range of different sensor modalities such as electroencephalography (EEG), electrooculogram (EOG), electromyography (EMG), electrocardiography (ECG), pulse oximetry, and respiratory signals. The EEG is the most critical modality, which is why most single-channel automatic sleep staging algorithms rely on a single (average) EEG channel. The configurations of EEG montages and the availability of other sensor modalities vary widely across datasets. The annotation process is formalized through American Academy of Sleep Medicine (AASM) guidelines [3] or Rechtschaffen and Kales (R&K) guidelines [4], and is usually performed for segments of 30 seconds, referred to as epochs. The assessment of an overnight PSG recording by a human expert is a tedious process, which requires up to several hours of work, and is subject to a high inter-rater variability [5, 6].

Prospects of automatic sleep staging: A study [7] evaluated machine-learning-based automated sleep staging models on PSG recordings scored by multiple human raters, using the consensus of these raters serving as the benchmark. The results demonstrated that automatic sleep staging not only significantly outperformed human raters in terms of accuracy but also exhibited higher Cohen's kappa values, indicating superior inter-rater reliability closer to the consensus of human raters. Even more striking, a recent study [8] showed that a deep learning-based algorithm for sleep staging, even when trained on datasets characterized by noisy labels produced by various

human raters adhering to the AASM guidelines, can achieve similar performance when trained on non-standard channel configurations and therefore does not require strict compliance with the AASM standards to achieve reliable performance. In fact, the inclusion of automatic sleep staging methods as part of the assessment protocol could mark a long overdue step towards an improvement of the standardization of the assessment procedure to reduce both inter-rater as well as inter-center variability [8]. This provides a clear incentive for the identification of robust and increasingly accurate model architectures generalizing across datasets and input configurations.

Rationale for this study: While the field of automatic sleep staging by means of machine learning has evolved a lot recently, compelling evidence on several important design decisions is lacking. First, there is no consensus on the most suitable input representation. State-of-the-art models from the literature typically rely on spectrograms as input representation, which, however, unlike the raw time series do not retain the full complexity of the input signal. Even though spectrograms encode a useful inductive bias, competitive models trained on raw time series hold the promise of eventually outperforming spectrogram-based models when (pre)trained on large datasets due to their ability to learn more nuanced representations. Second, even for a given input representation architectural design choices have rarely been investigated systematically. Most notably, beyond the predominantly used recurrent neural networks[9] and most recently transformer models[10], such an investigation should include structured state space sequence (S4) models, which are well-known for their ability to capture long-range dependencies in time series data [11] and have been successfully applied to other physiological time series data, such as electrocardiography data [12].

Technical contributions: We summarize the main contributions of this work as follows:

- (1) At the example of sleep staging, we devise a systematic procedure to identify optimal model architectures for long time series annotation tasks within the search space of encoder-predictor architectures, which encompasses most literature approaches.
- (2) Building on this procedure, we identify optimal model architectures for both raw time series and spectrograms as input, as well as for single-channel and multi-channel configurations, which outperform literature approaches on the Sleep EDF dataset—a widely-used public medium-sized benchmark dataset for sleep staging—and, most notably, on the large-scale Sleep Heart Health Study dataset when trained without any further hyperparameter ad-

justments. This underscores the robustness of our findings.

(2.1) For both raw time series and spectrogram input representations, we identify structured state space models as very effective sequence encoders albeit with input-modality-specific preprocessing (operating directly on spectrograms vs. operating on time series representations encoded through a shallow CNN).

(2.2) Optimal predictor models aggregating epoch-level predictions also depend on the chosen input representation (S4 model for raw time series input, transformer model for spectrogram input) stressing the importance of devising a structured procedure to identify such optimal model architectures.

2. Methods

2.1. Related Work

Machine learning and in particular deep learning algorithms have improved tremendously in the past few years. Recently, algorithms have a level of performance on par within the range of human inter-rater variability [7]. While most approaches still follow a purely supervised training procedure, self-supervised pretraining is considered increasingly often to learn representations from unlabeled data [13, 14] before finetuning on labeled data. Models operate on time-domain input, frequency-domain input, or combinations of both [15]. The sleep staging task is typically framed as a sequence task, where multiple epochs, i.e., episodes of 30 seconds, of input signal in the chosen input representation are mapped to a sequence sleep stage annotation, one per input epoch.

Encoder-predictor models: Most literature approaches can be categorized as encoder-predictor models. The encoder extracts local features, which typically get reduced to one output token per input epoch, while the predictor aggregates local features according to the temporal context [16], see Figure 1 for a schematic representation. Such architectures are also preferable on general grounds as they implement the principle of scale separation [17] and hierarchical representations [18, 19].

Unifying literature approaches: In Table 1, we we categorize literature approaches according to the used model components. First of all, the table demonstrates that the class of encoder-predictor models is a very broad class encompassing the majority of literature approaches. The most notable model architecture from the literature that does not fall into the category of encoder-predictor models in the above sense is the U-Sleep model [20],

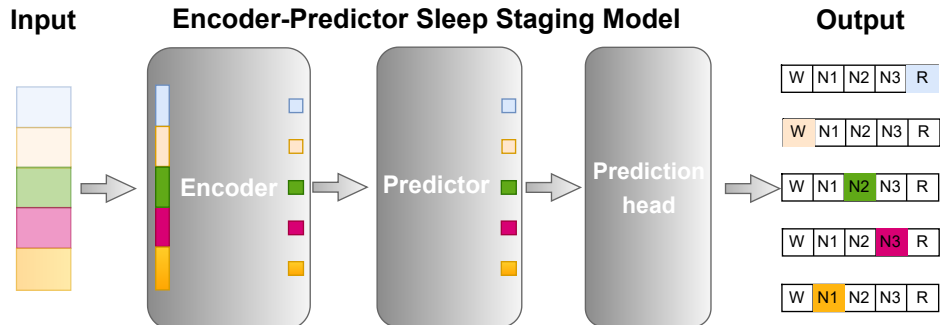


Figure 1: Schematic representation of the encoder-predictor architecture for sleep staging models.

which instead relies on a U-net architecture, and single-epoch models such as [21, 22]. Second, encoder and predictor models are often chosen identically, as for example in the case of (L-)SeqSleepNet [23], SleepTransformer [24] or RobustSleepNet [25]. The predominant choice are recurrent neural networks [16, 15, 25, 23], while recently also transformer models have been explored [24]. The pooling operation to reduce the temporal resolution of the encoder representation is often realized through an attention mechanism.

name	input	encoder	pooling	predictor	remarks
S_4 Sleep(ts)	raw	CNN+S4	average	S4	this work
S_4 Sleep(spec)	spec	S4	average	transformer	this work
L-SeqSleepNet[23]	spec	LSTM	folding	LSTM	long sequence input
ProductGraphSleepNet[26]	de	GCN (as both encoder and	pooling)	GRU	graph based
SAGSleepNet [27]	spec	GCN	average	GRU	graph based
SleepTransformer[24]	spec	Transformer	attention	Transformer	
XSleepNet1 [15]	raw+spec	raw:CNN spec: FB	attention	raw:GRU spec: LSTM	dual modality input
XSleepNet2 [15]	raw+spec	raw:CNN spec: FB	attention	raw:GRU spec: LSTM	dual modality input
RobustSleepNet [25]	spec	channel-attention + GRU	attention	GRU	
IITNet [28]	raw	Resnet	-	LSTM	sub-epoch encoder
SeqSleepNet [16]	spec	FB+LSTM	attention	LSTM	
DeepSleepNet [29]	raw	CNN	max	LSTM	

Table 1: Unifying encoder-predictor approaches for sleep staging from the literature and this work. (FB: filter bank layer that is composed of restricted fully connected layer. Dconv: dilation convolution layer. GCN: graph convolutional network. raw: raw time series. spec: spectrograms. de: differential entropy. folding: folding subnetwork)

2.2. Models

Encoder-Predictor Model: We follow the design choice of encoder-predictor models introduced above, which we describe here at a higher level of detail:

Roughly speaking, the raw input (either raw time series or spectrograms) is processed by an encoder model, which typically returns a semantically enriched, temporally downsampled representation. The conventional approach in the field is to reduce the temporal resolution to a single token per sleep staging epoch but it is also possible to chose a temporally more finegrained (sub-epoch) resolution [28] for the intermediate representation. Consequently, this representation is passed to the predictor model, which integrates the information across tokens on the epoch or sub-epoch-level. Finally, the output of the predictor model is processed by a prediction head to produce epoch-level predictions. In the case of an epoch-level encoder, this can be as simple as a MLP or a single linear layer shared across all output tokens. In the case of a sub-epoch-level encoder, it will typically be preceded by a local pooling layer to reach an output representation that matches the required temporal resolution at epoch-level.

Modular design: Different encoder and predictor architectures can be mixed in a modular fashion. One of the core contributions of this work is to provide a structured assessment of their different components and their interplay. Beginning with an exploration of single-epoch prediction models facilitates the identification of superior architectural designs adept at abstracting high-quality, epoch-level representations. This initial step is crucial for pinpointing encoder architectures highly effective for multi-epoch models. Subsequently, multi-epoch prediction models that adept at leveraging long-range dependencies, a capability, pivotal for significantly enhancing sleep staging accuracy and reliability, are identified by searching the architectural design space. Below, we provide very brief descriptions of the different architectural components considered in our experiments in order not to obstruct the flow of reading. More detailed descriptions are provided in Appendix A in the supplementary material and in the accompanying code repository [30].

2.2.1. Single-epoch prediction models

Single-epoch encoders: As single-epoch encoder, we consider shallow CNN encoders or passing the input directly to the predictor. Using a shallow CNN is a commonly used design choice both for raw waveform and for spectrogram-based audio processing, see for example [31, 32] as it allows map the raw input to more favorable input representation for the predictor, while adding little complexity and optionally (in the cases of strided convolutions) reducing the temporal resolution of the signal.

- time series input:
 - *CNN*: two layers of strided 1d convolutions interleaved with ReLU activations
 - *NONE*: identity function
- spectrogram input:
 - *CNN*: reshaping of frequency and channel axes into a single axis followed by two layers of 1d convolutions interleaved with GeLU activations as generalization of the whisper encoder [32] to multiple input channels
 - *NONE*: reshaping of frequency and channel axes into a single axis

Single-epoch predictors: As epoch encoder we consider a bidirectional LSTM model as representative for the predominantly used recurrent neural network predictors in addition to transformer and structured state space sequence (S4) models.

- *LSTM*: two-layer bidirectional LSTM model
- *TF*: four-layer transformer model
- *S4*: four-layer S4 model

Single-epoch prediction heads: To keep the scope of the study limited, we only explore global/local average pooling layers followed by a linear layer with five output neurons.

2.2.2. Multi-epoch prediction models

Multi-epoch encoders: For multi-epoch input, we consider different strategies. First, we consider so-called epoch encoder, corresponding to identified optimal single-epoch prediction models (*EES₄* and *EENS₄*). In the case of raw time series input we also consider a shallow CNN with large strides to provide a temporally downsampled hidden representation (SCNN). Spectrograms as input modality are already heavily downsampled compared to the original time series as input. This enables to directly use the encoders from the single-epoch case (*CNN* and *NONE*) without further internal aggregation.

- time series input:
 - *EES₄*: *CNN* encoder with *S₄* predictor and average pooling as epoch encoder
 - *SCNN*: four layer of strided 1d convolutions interleaved with ReLU activations with temporal downsampling factor of 100 inspired by the wav2vec2 encoder for raw audio data [31]
- spectrogram input:
 - *EEENS₄*: *NONE* encoder with *S₄* predictor and average pooling as epoch encoder
 - *CNN*: using the single-epoch *CNN* encoder for spectrograms as input without any aggregation on epoch level
 - *NONE*: using *NONE* defined as single-epoch encoder

Multi-epoch predictors: We consider the same predictors as in the single-epoch prediction models.

Multi-epoch prediction heads: We consider the same prediction heads as in the single-epoch prediction models.

2.3. Datasets

Sleep-EDF (SEDF): The SEDF database comprises 197 sleep recordings, sourced from two specific subsets: the Sleep Cassette (SC), which includes 153 recordings from 78 healthy individuals, and the Sleep Telemetry (ST), featuring 44 recordings from 22 patients experiencing mild difficulties in falling asleep. All recordings include Fpz-Cz and Pz-Oz EEG channels, as well as EOG channels, all sampled at 100 Hz. The recordings are manually scored into wake stage (W), NREM stages (N1-N4), rapid-eye-movement stage (REM), MOVEMENT and UNKNOWN according to the R&K guidelines. Following the common preprocessing in the literature, we merged N3 and N4 (into N3), and excluded data segments labeled as MOVEMENT and UNKNOWN. We conducted experiments on multi-channel data containing two EEG channels (Fpz-Cz and Pz-Oz) and one EOG channel (horizontal), as well as on single-channel data consisting only of the Fpz-Cz EEG channel. We investigate both single- as well as multi-channel inputs to compare as broadly as possible to available literature results. We performed a random split of the recordings, allocating 80% of the recordings for training, 10%

for validation and 10% for testing. As no standard splits are available in the literature, we release our splits for later reproducibility [30]. A selective subset of the Sleep Cassette (SC) subset, designated as SEDF20 in this work, comprising 39 polysomnography (PSG) recordings from 20 subjects (10 males and 10 females) aged between 25 and 34, is frequently utilized in studies focusing on automatic sleep staging. To facilitate a meaningful comparison of the outcomes of our study with existing literature, we also conducted experiments with our final selected models on this specific subset. **SHHS:** The Sleep Heart Health Study (SHHS) dataset includes polysomnography data collected from participants across two overnight visits (Visit 1 and Visit 2), with several intervening years for follow-up [33, 34]. The dataset is available for download and usage through the National Sleep Research Resource (NSRR) platform [35], following a user registration process and agreement to abide by specific data use policies. For our study, we utilized data from SHHS Visit 1, which includes two EEG channels, two EOG channels, and one EMG channel, among other signals. The recordings are manually scored according to the R&K guidelines. For comparability with literature approaches [23], recordings that did not include all stages—wake (W), NREM stages N1 through N4, and REM—were excluded. This resulted in the retention of 5463 recordings. As with SEDF, we merged N3 and N4, and excluded data segments labeled as MOVEMENT and UNKNOWN. The dataset was resampled to 100 Hz. We conducted experiments on multi-channel data containing two EEG channels (C4-A1 and C3-A2), two EOG channels (left and right), and one EMG channel, as well as on single-channel data consisting only of the C4-A1 EEG channel. We performed a random split of the recordings, allocating 70% of the recordings for training and 30% for testing, following the split ratio used in [23]. Additionally, we set aside 100 recordings from the training set specifically for validation purposes. Again, we release these splits for later reproducibility as part of the accompanying code repository [30].

Rationale for dataset selection: We selected the two datasets with significantly different sizes to serve our research purposes effectively. The medium-sized SEDF allowed us to conduct the entire training-testing process for dozens of different models throughout the model selection phase. This comprehensive evaluation, encompassing a broad range of models and hyperparameter settings, would have been infeasible on the much larger SHHS dataset. Secondly, and equally important, utilizing both SEDF and SHHS datasets allowed us to rigorously test the generalizability of our models across

Dataset	Recordings	Patients	Included channels
SEDF(full) [36, 37]	197	100	EEG (Fpz-Cz*, Pz-Oz), EOG (horizontal)
SEDF20 [36, 37]	39	20	EEG (Fpz-Cz*, Pz-Oz), EOG (horizontal)
SHHS Visit 1 [33, 34]	5463	5463	EEG (C3-A2, C4-A1*), EOG (left, right), EMG

Table 2: Summary of datasets used in this study (*: selected channel for single-channel configuration experiments)

diverse data sources. This approach mitigates the risk of overfitting to a specific dataset, thereby ensuring our findings are robust and applicable to various clinical settings and populations.

Preprocessing: Both datasets were used in terms of two different input representations, raw time series and spectrograms. Spectrograms were generated in a manner consistent with L-SeqSleepNet [23]. Each channel signal from a 30-second epoch was transformed to generate a log-magnitude time-frequency image. This involved dividing the signal into 29 time steps and 129 frequency bins using the short-time Fourier transform (STFT) with a window length of 2 seconds and a 1 second overlap. A Hamming window and a 256-point fast Fourier transform (FFT) were used in the process. The resulting amplitude spectrum for each channel underwent logarithmic transformation, creating a time-frequency image. The raw time series input underwent no further preprocessing.

2.4. Training procedure and performance evaluation

Training: To mitigate issues due to imbalanced label distributions that are typical for this task, we use focal loss [38] as loss function. For all experiments, we use a fixed effective batch size of 64 achieved through gradient accumulation. We performed experiments with learning rates determined via the learning rate finder [39] as well as with a fixed learning rate of 0.001 for each experiment. The learning rate yielding superior validation set performance was selected. We train models using a constant learning rate using AdamW [40] as optimizer. For training and validation, we divide the whole input sequence of a given sample into consecutive segments whose lengths coincide with the model’s input size. For SEDF, the models underwent training for 50 epochs, with validation performed after each training epoch. For

SSHS, we found longer training beneficial (in terms of training iterations) and train for 30 epochs. For the final test set evaluation, we select the model at the training epoch with the best validation set performance (in terms of macro- F_1 score, introduced in detail below). We train on non-overlapping crops of the specified input size. During test time, we split the input sequences into segments of the same length but use a smaller stride length coinciding with the length of a single epoch. For most segments, we obtain in this way multiple predictions corresponding to different positions in the input sequence passed to the model. We subsequently average all available predictions on the level of output probabilities for a given segment.

Performance: Irrespective of the input size, the procedure described in the previous section yields a probabilistic model prediction per test/validation set epoch. We can then compare dichotomized model predictions with the ground truth. The most commonly used metric in the field is the macro- F_1 -score, computed as the mean of the individual label F_1 -scores,

$$\text{macro } F_1 = \frac{1}{5} \sum_{c \in C} F_{1,c}, \quad (1)$$

where $C = \{W, N1, N2, N3, REM\}$ and $F_{1,c}$ is the F_1 score for class c . The macro F_1 score serves as primary target metric in the sense that also model selection on the validation score is carried out based on this metric. For informativeness, we report a range of other metrics but stress that the models have not been specifically optimized towards these metrics. In particular, we report the individual label F_1 scores that constitute the macro F_1 score and the overall prediction accuracy but rush to add that the use of accuracy as target metric is problematic in the presence of label imbalance and therefore most sensitive to the performance on the majority class of NREM class N2. Finally, we also report the macro average of the area under the receiver operating curve (AUROC) defined as

$$\text{macroAUROC} = \frac{1}{5} \sum_{c \in C} \text{AUROC}_c, \quad (2)$$

where $C = \{W, N1, N2, N3, REM\}$ and AUROC_c denotes the area under the receiver operating curve for class c , considering class c as positive and the remaining classes as negative classes. This is one example for a commonly used scoring metric that is based on (the ranking of) output probabilities rather

than dichotomized outputs and therefore adds complementary information compared to metrics of the latter category.

Score estimation: We base our most reliable experiments on SEDF(full) dataset and the SHHS dataset on a simple holdout set evaluation scheme. The only exception from this approach is the small-scale SEDF20 subset, where we use a leave-one-patient-out cross-validation scheme in order to conform with predominantly used evaluation scheme in the literature. For full transparency, we indicate the precise dataset choice as well as score estimation method for all considered methods in the final results in Table 5.

Predictive uncertainty during model selection: An uncertainty estimate for the achieved results is very desirable already during model selection to assess the significance of the performance differences. There are two main sources of uncertainty that are of main interest: the uncertainty in the final score due to the randomness of the training process and the uncertainty due to the finiteness and particular composition of the test/validation set. The former uncertainty is typically assessed through multiple training runs. For computational reasons, we resort to a single training run at this stage and defer a proper assessment to the evaluation in Section 3.3. However, we can assess the second kind of uncertainty through (empirical) bootstrapping ($n = 1000$ iterations) on the test set. To determine if the difference in performance (according to macro-F1 score as metric) is significant, we calculate 95% confidence intervals for the score difference. If the confidence interval for the performance difference does not overlap with zero, we regard the performances of the two models as statistically significantly different.

Predictive uncertainty during final model evaluation: To assess the systematic uncertainty due to the randomness of the training process, we perform three training runs per scenario and report the median F_1 -score as well as the interquartile ranges as fluctuation measure. We estimate the statistical uncertainty due to the finiteness and composition of the test set through empirical bootstrapping ($n = 1000$ iterations) on the test set. We report the median of the three bootstrap uncertainty measures across the three training runs. We report the final results in the form (median macro – F_1) \pm (systematic uncertainty) \pm (statistical uncertainty). To assess the statistical significance of performance differences while also incorporating the uncertainty due to the randomness of the training process, we follow the methodology proposed in [41]. Three training runs for model A and model B yield in total 9 combination. By bootstrapping the score difference as described above, we can assess the statistical significance of the score difference

between pairs of models individually. Now we set a threshold, relating to the willingness to accept fluctuations due to the randomness of the training process, and declare model A superior to model B if the fraction of pairwise tests with significant outcomes exceeds the predetermined threshold. As in [41], we use a threshold of 60%.

3. Results

Organization of experiments: In Figure 2, we provide an overview over the course of the experiments. We proceed in two stages: To restrict the search space, we start in a first stage in Section 3.1 by considering models that take a single epoch as input. Based on the insights of this experiment, we proceed in Section 3.2 to multi-epoch models leveraging the optimal model architectures identified in the first step as epoch encoders. In this second phase, we strive to identify optimal encoder and predictor combinations both for raw time series and spectrograms as input. Finally, we investigate whether the identified models can profit from sub-epoch as apposed to full-epoch encoders. We only report validation set performances at this point to avoid overfitting to the SEDF test set. We conclude the results part with Section 3.3, where we put the identified model architectures to a test on two different subsets of SEDF. To validate the robustness of our findings, we also test the identified model architectures on the different dataset, the large-scale SHHS dataset.

3.1. Model selection: single-epoch models

For single epoch models, we assess the impact of the predictor model (S_4 , TF , $LSTM$). For both input representations, we consider convolutional encoders (CNN) as well as no encoder ($NONE$). All results are compiled in Table 3. The results for raw time series as input both for single- as well as multi-channel clearly distinguish $CNN+S_4$ as best-performing architecture. For time series input, a CNN encoder turns out to be beneficial as compared to using no encoder. On the contrary, for spectrogram data, using no encoder turns out to be the more favorable choice. These results suggest that the architectural choices are inherently tied to the input representations. The difference between both encoder choices for identical predictor model is most strongly pronounced for S_4 as predictor, whereas TF is barely influenced by this choice. The best-performing model on spectrogram input according macro- F_1 score turns out to be $NONE+S_4$, again across both

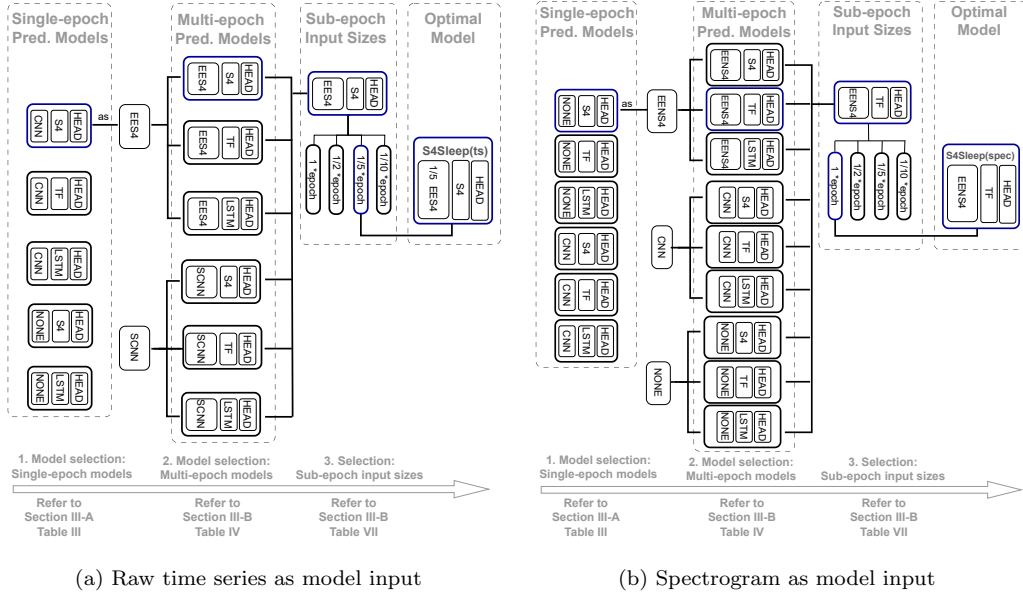


Figure 2: Flow chart demonstrating the organization of the experiments that lead to the identification of optimal model architectures for (a) raw time series and (b) spectrograms as input. Both start by identifying strong single-epoch models, which are then leveraged (in the form of epoch encoders) to explore multi-epoch prediction models (while also exploring alternative encoder choices). Finally, for the two identified architectures the usage of sup-epoch instead of full-epoch encoders is explored. Afterwards the two best-performing model architectures, $S_4Sleep(ts)$ and $S_4Sleep(spec)$, are evaluated on held-out test sets and retrained on the commonly used SEDF20 and the large-scale SHHS dataset, leading to the final performance evaluation compiled in Table 5.

channel settings. Looking at overall best performance, raw-time-series-based models are outperformed by spectrogram-based models for multi-channel input while the opposite ordering is observed in the single-channel case. In line with expectations, multi-channel input seems to exhibit a systematic positive effect compared to single-channel input. We use these insights from the single-epoch case to construct multi-epoch prediction models using the identified encoder-predictor combinations as epoch encoders.

3.2. Model selection: multi-epoch models

Time series input: For raw time series, we consider the best-performing encoder-predictor combination ($CNN+S_4$) from the previous sections as epoch encoder (EES_4) in combination with the three different predictor architectures (S_4 , TF and $LSTM$) introduced earlier. In addition, we investigate a

channels	features	encoder	predictor	F_1 (\uparrow)						acc.	macro
				macro	W	N1	N2	N3	REM	(\uparrow)	AUC (\uparrow)
EEG \times 2 EOG \times 1	raw	CNN	S4	0.780	0.916	0.489	0.851	0.822	0.824	0.823	0.961
		CNN	TF	0.745	0.913	0.439	0.811	0.802	0.760	0.793	0.950
		CNN	LSTM	0.767	0.917	0.482	0.840	0.807	0.787	0.813	0.957
		NONE	S4	0.776	0.910	0.510	0.837	0.802	0.821	0.813	0.960
		NONE	LSTM	0.729	0.903	0.412	0.810	0.792	0.728	0.778	0.942
	spec	CNN	S4	0.750	0.914	0.433	0.830	0.773	0.802	0.808	0.951
		CNN	TF	0.775	0.911	0.488	0.844	0.798	0.833	0.817	0.956
		CNN	LSTM	0.771	0.920	0.453	0.842	0.806	0.836	0.821	0.955
		NONE	S4	0.783	0.915	0.510	0.851	0.802	0.836	0.822	0.960
		NONE	TF	0.777	0.915	0.494	0.850	0.799	0.827	0.822	0.961
EEG \times 1	raw	CNN	S4	0.749	0.908	0.421	0.841	0.811	0.762	0.803	0.954
		CNN	TF	0.710	0.880	0.355	0.822	0.818	0.675	0.770	0.954
		CNN	LSTM	0.744	0.902	0.403	0.852	0.821	0.744	0.802	0.951
		NONE	S4	0.743	0.897	0.454	0.829	0.799	0.734	0.786	0.947
		NONE	LSTM	0.714	0.887	0.396	0.831	0.801	0.653	0.770	0.938
	spec	CNN	S4	0.695	0.855	0.400	0.810	0.766	0.646	0.744	0.931
		CNN	TF	0.723	0.882	0.386	0.836	0.784	0.726	0.782	0.942
		CNN	LSTM	0.730	0.882	0.410	0.832	0.797	0.728	0.785	0.944
		NONE	S4	0.734	0.884	0.417	0.831	0.796	0.742	0.787	0.949
		NONE	TF	0.721	0.873	0.415	0.830	0.785	0.701	0.769	0.942
		NONE	LSTM	0.715	0.867	0.362	0.832	0.798	0.717	0.775	0.937

Table 3: Comparing different encoder and predictor architectures for a *single epoch input size* trained on SEDF based on validation set scores. Best results for a given channel configuration are marked in bold face and outperform all competing alternatives in a statistically significant manner. The analysis identifies S4 models as best predictor architecture (in combination with a shallow CNN encoder for raw time series and without any encoder for spectrogram input).

strided convolutional encoder (*SCNN*) in combination with these three predictors. Finally, we also consider the case of matching epoch encoder and predictor architectures (*EETF+TF* and *EELSTM+LSTM*). We summarize the results of our experiments for 15 epochs input in Table 4. *EES₄+S₄* is clearly singled out as the top-performing architecture, with a significant gap to the second-best combinations *EES₄+TF* in the multi-channel setting and *SCNN+TF* in the single-channel setting.

Spectrogram input: As in the case of raw time series input, we consider an epoch encoder built from the best-performing encoder-predictor combination (*NONE+S₄*) identified in the single-epoch experiment *EENS₄* in addition to the already known encoders from the single-epoch case, CNN and *NONE*.

channels	features	encoder	predictor	F_1 (\uparrow)					acc. (\uparrow)	macro AUC (\uparrow)	
				macro	W	N1	N2	N3			REM
EEG \times 2 EOG \times 1	raw	EES4	S4	0.820	0.931	0.612	0.862	0.798	0.895	0.851	0.973
		EES4	TF	0.812	0.931	0.563	0.864	0.815	0.888	0.851	0.972
		EES4	LSTM	0.803	0.925	0.538	0.862	0.818	0.871	0.843	0.969
		SCNN	S4	0.787	0.919	0.515	0.840	0.809	0.854	0.830	0.964
		SCNN	TF	0.804	0.922	0.546	0.865	0.817	0.872	0.844	0.969
		SCNN	LSTM	0.795	0.922	0.537	0.860	0.786	0.870	0.840	0.968
	spec	EENS4	S4	0.811	0.928	0.556	0.867	0.818	0.886	0.851	0.970
		EENS4	TF	0.815*	0.928	0.578	0.857	0.827	0.884	0.846	0.970
		EENS4	LSTM	0.815*	0.931	0.563	0.865	0.824	0.892	0.853	0.969
		CNN	S4	0.788	0.913	0.542	0.848	0.774	0.864	0.829	0.963
		CNN	TF	0.788	0.909	0.506	0.854	0.801	0.872	0.832	0.966
		CNN	LSTM	0.799	0.924	0.545	0.862	0.789	0.876	0.844	0.968
		NONE	S4	0.815*	0.930	0.558	0.863	0.823	0.898	0.853	0.969
		NONE	TF	0.782	0.913	0.479	0.847	0.808	0.864	0.828	0.961
NONE	LSTM	0.789	0.913	0.520	0.856	0.792	0.863	0.832	0.961		
EEG \times 1	raw	EES4	S4	0.801	0.913	0.569	0.868	0.801	0.853	0.839	0.970
		EES4	TF	0.763	0.905	0.472	0.845	0.813	0.781	0.813	0.961
		EES4	LSTM	0.770	0.911	0.480	0.853	0.815	0.790	0.822	0.963
		SCNN	S4	0.786	0.909	0.504	0.857	0.819	0.841	0.833	0.965
		SCNN	TF	0.789	0.916	0.497	0.867	0.813	0.851	0.840	0.967
		SCNN	LSTM	0.781	0.916	0.506	0.866	0.757	0.869	0.834	0.966
	spec	EENS4	S4	0.784	0.897	0.530	0.866	0.784	0.842	0.827	0.962
		EENS4	TF	0.797	0.911	0.536	0.865	0.812	0.861	0.839	0.968
		EENS4	LSTM	0.790	0.904	0.549	0.858	0.798	0.843	0.832	0.965
		CNN	S4	0.764	0.889	0.472	0.848	0.787	0.821	0.810	0.956
		CNN	TF	0.779	0.898	0.481	0.859	0.808	0.847	0.828	0.960
		CNN	LSTM	0.780	0.905	0.491	0.859	0.798	0.846	0.827	0.963
		NONE	S4	0.777	0.891	0.501	0.861	0.803	0.828	0.824	0.962
		NONE	TF	0.741	0.876	0.438	0.840	0.783	0.767	0.789	0.950
NONE	LSTM	0.739	0.874	0.441	0.839	0.767	0.773	0.791	0.945		

Table 4: Comparing different encoder and predictor architectures for *15 epochs input size* trained on SEDF(full) based on validation set scores. The scores marked with an asterisk (*) represent models whose scores do not exhibit statistically significant differences (according to macro- F_1 score) compared to the best-performing model of the respective channel and input-modality combination. The remaining notation follows Table 3. The experiments identify an S4-model-based epoch encoder (EES4) in combination with an S4-model-based predictor as best-performing model for time series input and an S4-model-based epoch encoder (EENS4) in combination with a transformer-model-based predictor as best-performing model for spectrogram input.

As before, we summarize the results of our experiments for 15 epochs input in Table 4. Both in the single-channel as well as in the multi-channel case, the epoch encoder EES_4 is clearly singled out as best-performing encoder architecture. Even though the input length of the predictor model is in the

case of epoch encoders identical to that of the corresponding predictor in the raw time series case, the S_4 does not turn out as strong as in the raw time series case. Interestingly, in the multi-channel case the three architectures $EENS_4+TF$, $EENS_4+LSTM$ and $NONE+S_4$, i.e. an architecture without epoch encoder, yield similar performance, the single-channel setting is clearly dominated by $EENS_4+TF$.

Comparative assessment: For time series as input, the EES_4 encoder represents the key component to achieve competitive performance, overall EES_4+S_4 turns out as best-performing combination. For spectrograms as input, as we are interested in identifying architectures that can generalize also to other datasets and channel configurations, we identify $EENS_4+TF$ (as opposed to $NONE+S_4$) as architecture of choice. It is worth noting the consistent performance gaps between the best-performing models operating on time series compared to those operating on spectrograms (0.820 vs. 0.815 for multi-channel and 0.801 vs. 0.797 for single-channel). As in the case of single epoch input models, we find a consistent improvement of multi-channel models over single-channel models.

Full-epoch vs. sub-epoch encoder: In addition to the encoders for single or multiple epochs as input, we also conducted experiments with sub-epoch-level encoders. We used $1/n$ of an epoch as input unit, which corresponds to n output tokens per input epoch after the encoder, and considered values for n of 2, 5, and 10 for the overall best-performing model architecture (EES_4+S_4). Notation-wise, we refer to a sub-epoch encoder with $n = 5$ as $1/5 EES_4$, for the case of a S_4 epoch encoder. The results shown in Table B.7 in the supplementary material suggest that the choice of sub-epoch level can influence the model performance. In the case of single-channel input, $n = 5$ exhibited superior performance in terms of macro- F_1 scores compared to the single-epoch encoder ($n = 1$). Even though the model performance is on par with the standard epoch encoder in the case of multi-channel input, we strive to identify architectures that work reliably across different situations and we therefore still select a sub-epoch encoder ($n = 5$) for our final experiments. In the case of spectrogram input, the multi-channel case favors both $n = 1$ and $n = 5$ but the single-channel case clearly distinguishes $n = 1$. As we are looking for an architecture that generalizes across channel configurations, we use the conventional epoch encoder ($n = 1$) in this case.

Summary: At this point we recapitulate the findings from the experiments presented in the previous paragraphs: For time series input, we identify $1/5 EES_4+S_4$, i.e., an epoch encoder leveraging a S_4 model operating on a sub-

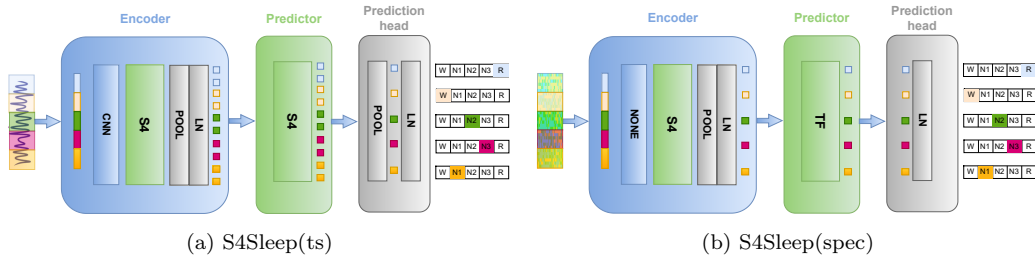


Figure 3: Schematic representation of the selected model architectures used in this work. (a) S4Sleep(ts): Raw time series as input modality (b) S4Sleep(spec): Spectrogram as input modality

epoch level of $1/5$ of an epoch combined with another S4 model as predictor, as best-performing architecture and refer to it as $S_4Sleep(ts)$. For spectrogram input, we identify $EENS_4+TF$, i.e., again an epoch encoder leveraging an S4-model internally but this time operating on the input directly combined with a transformer predictor model, as best-performing architecture and call it $S_4Sleep(spec)$. The two selected model architectures are summarized schematically in Figure 3.

3.3. Performance evaluation

Overview: In this section, we put the identified architectures $S_4Sleep(ts)$ and $S_4Sleep(spec)$ to a test. First, we evaluate the identified optimal model architectures for multi-channel and single-channel input on the SEDF(full) test set. Second, we also provide results on the smaller SEDF20 subset, which is one of the most widely used benchmark dataset for sleep staging. Finally, as the whole analysis so far concentrated on SEDF, we aim to demonstrate that the identified architectures also generalize to other (large-scale) datasets after retraining. To this end, we trained and evaluated the same model architectures with identical hyperparameters (except for the learning rate, which was determined using the learning rate finder as described above).

Performance on SEDF(full): The results achieved on SEDF(full) are summarized in Table 5. As a general observation, the proposed S4Sleep methods represent the best-performing methods in both the single-channel and multi-channel categories. Surprisingly, however, the time series-based $S_4Sleep(ts)$ performs best in the single-channel case, while the spectrogram-based $S_4Sleep(spec)$ excels in the multi-channel case. As an interesting observation, $S_4Sleep(spec)$ does not show a competitive score in comparison

to $S4Sleep(ts)$ in the single-channel case, while it still performs on par with literature approaches within statistical error bars. Disregarding the fact that literature approaches differ slightly in sample selection, splits and score evaluation methods and assuming that the scores of the literature approaches are subject to similar statistical and systematic errors as the proposed models, the proposed respective best-performing models outperform all literature approaches in a statistically significant manner.

Performance on SEDF20: In order to allow for a comprehensive comparison to literature approaches, we include results on the smaller SEDF20 subset using a leave-one-patient-out cross-validation scheme, aligning with the most widely used evaluation procedure in the literature. While the performance insights from this subset may be less reliable due to its smaller size and more homogeneous patient collective, it’s important to stress that this limitation applies equally to all studies utilizing this dataset. This approach is specifically chosen to improve comparability with existing literature, ensuring that our findings are directly comparable to those of other researchers working under similar constraints. The internal ranking of the two approaches $S4Sleep(ts)$ and $S4Sleep(spec)$ agrees with that on the full SEDF dataset. The scores on SEDF20 are generally higher than those on the full SEDF, most likely due to a more homogeneous underlying patient collective. In the case of a single input channel, $S4Sleep(ts)$ is only outperformed by $XSleepNet2$, while still remaining competitive with the best-performing results within error bars. For multi-channel input, $S4Sleep(spec)$ represents the best-performing solution but the advantage over $XSleepNet2$ is most likely not statistically significant. Due to the nature of the cross-validation procedure, the model will also be evaluated on samples that have been placed in the validation set of the full SEDF dataset during the model selection procedure, which might lead to a slight overestimation of the generalization capabilities of the proposed models. In addition, we only provide mean statistical errors computed from respective statistical errors on the respective folds, but no systematic errors across several training runs. This turns the results on SEDF20 less reliable than those on full SEDF and SHHS. The close proximity of the literature results represents a challenge for statically significant model comparison, putting into question the use of SEDF20 as primary benchmarking dataset for sleep staging algorithms.

Performance on SHHS: The extensive SHHS dataset, previously unseen during the model selection procedure, serves as an objective evaluate the robustness of our findings. Although existing literature often lacks detailed

disclosure regarding dataset divisions, the substantial volume of the SHHS dataset substantially diminishes the impact of this variability on the comparability of results. Our findings demonstrate minimal variation in performance, underscoring the robustness and reliability of our model. To foster greater transparency and reproducibility in research, we have provided details of our dataset split. First of all, it is noticeable from the SHHS results presented in Table 5 that both $S4Sleep(ts)$ and $S4Sleep(spec)$ models outperform the current state-of-the-art performance for both considered channel configurations. In contrast to the majority of literature approaches, we provide statistical and systematic uncertainty estimates. Both are on the order of 0.001 and therefore comparably small, which underlines the robustness of our results. Unfortunately, no error estimates for the literature results are available. However, under the assumption that the literature results are subject to comparable statistical error estimates as the proposed approaches, $S4Sleep(ts)$ would not overlap with the best $L-SeqSleepNet$ -performance, which would represent a significant improvement in performance in the single-channel case. In the multi-channel case the performance difference between the best-performing $S4Sleep(spec)$ with a macro- F_1 score of 0.832 in comparison to the score of $XSleepNet2$ with a macro F_1 score 0.823 and, again under the assumption of comparable statistical uncertainties of the literature results, clearly significant. At this point one has to bear in mind that there is presently no generally agreed train-test split available on SHHS, a shortcoming that we aim to address by providing train-test splits as part of the code repository [30] accompanying this submission. On one hand, this means that scores are, strictly speaking, not directly comparable. On the other hand, SHHS is already a large-scale dataset, where score fluctuations due to the size of the test set are not expected to play a major role. This is argument is supported by the comparably small statistical uncertainties demonstrated in our analysis. As a final remark, it is worth stressing that the exceptionally strong performance of both $S4Sleep$ variants without further hyperparameter adjustments is a very good sign for the generalization capabilities of the proposed architecture, which will therefore be interesting to explore on other datasets and even in entirely different data modalities.

4. Discussion

Search for model architectures: This paper demonstrates the technical feasibility of identifying optimal model architectures from a rather large class

Table 5: Performance of selected models on SEDF(full), SEDF20 and SHHS (test set scores). Notation as in Table 4.

data model		channel	F_1 (\uparrow)					acc.	macro	
set			macro					(\uparrow)	AUC	
			W	N1	N2	N3	REM		(\uparrow)	
SEDF(full)	XSleepNet1 ^{c, k} [15]	single	0.778	-	-	-	-	-	0.836	-
	XSleepNet2 ^{c, k} [15]	single	0.779	-	-	-	-	-	0.840	-
	SleepTransformer ^{c, k} [24]	single	0.743	0.917	0.404	0.843	0.779	0.772	0.814	-
	S4Sleep(ts) ^{a, n}	single	0.796±0.004±0.004	0.925	0.503	0.854	0.839	0.855	0.839	0.958
	S4Sleep(spec) ^{a, n}	single	0.777±0.004±0.003	0.918	0.505	0.837	0.791	0.834	0.824	0.962
	XSleepNet1 ^{c, k} [15]	multi	0.774	-	-	-	-	-	0.840	-
	XSleepNet2 ^{c, k} [15]	multi	0.777	-	-	-	-	-	0.840	-
	RobustSleepNet ^{c, j} [25]	multi	0.763	-	-	-	-	-	-	-
	RobustSleepNet ^{a, j} [25]	multi	0.778	-	-	-	-	-	-	-
	U-Sleep ^{c, q} [20]	multi	0.79	0.93	0.57	0.86	0.71	0.88	-	-
	SAGSleepNet ^{a, l} [27]	multi	0.744±0.052	-	-	-	-	-	0.807	0.951
	S4Sleep(ts) ^{a, n}	multi	0.804±0.002±0.003	0.925	0.568	0.847	0.826	0.863	0.841	0.961
	S4Sleep(spec) ^{a, n}	multi	0.808±0.004±0.002	0.930	0.573	0.848	0.819	0.866	0.843	0.962
SEDF20	DeepSleepNet ^{b, l} [29]	single	0.769	0.847	0.466	0.859	0.848	0.824	0.820	-
	SeqSleepNet ^{b, l} [16]	single	0.786±0.002	0.912	0.447	0.880	0.862	0.830	0.856	-
	IITNet ^{b, l} [28]	single	0.776	0.877	0.434	0.898	0.848	0.824	0.820	-
	XSleepNet1 ^{b, l} [15][23]	single	0.800	0.913	0.495	0.880	0.869	0.842	0.860	-
	XSleepNet2 ^{b, l} [15][23]	single	0.806	0.922	0.518	0.880	0.868	0.839	0.863	-
	An et al 2022 ^{d, l} [21]	single	0.801	-	-	-	-	-	0.931	-
	L-SeqSleepNet ^{b, l} [23]	single	0.793±0.004	0.916	0.453	0.885	0.862	0.852	0.863	-
	S4Sleep(ts) ^{b, l}	single	0.804±0.004	0.922	0.522	0.894	0.877	0.877	0.876	0.977
	S4Sleep(spec) ^{b, l}	single	0.780±0.005	0.910	0.475	0.873	0.876	0.849	0.843	0.975
	XSleepNet1 ^{b, l} [15]	multi	0.798	-	-	-	-	-	0.852	-
	XSleepNet2 ^{b, l} [15]	multi	0.809	-	-	-	-	-	0.864	-
	RobustSleepNet ^{b, j} [25]	multi	0.791	-	-	-	-	-	-	-
	ProductGraphSleepNet ^{b, l} [26]	multi	0.774	0.886	0.426	0.874	0.847	0.834	0.838	-
	S4Sleep(ts) ^{b, l}	multi	0.805±0.004	0.911	0.536	0.893	0.857	0.892	0.873	0.978
	S4Sleep(spec) ^{b, l}	multi	0.810±0.004	0.912	0.525	0.894	0.858	0.871	0.870	0.979
SHHS	SeqSleepNet ^{f, p} [16]	single	0.802	0.918	0.491	0.882	0.835	0.882	0.872	-
	IITNet ^{f, o} [28]	single	0.798	0.901	0.481	0.884	0.852	0.872	0.867	-
	XSleepNet1 ^{f, p} [15]	single	0.807	0.916	0.514	0.885	0.850	0.884	0.876	-
	XSleepNet2 ^{f, p} [15]	single	0.810	0.920	0.499	0.883	0.850	0.882	0.875	-
	SleepTransformer ^{f, p} [24]	single	0.801	0.922	0.461	0.883	0.852	0.886	0.877	-
	L-SeqSleepNet ^{f, p} [23]	single	0.814	0.931	0.511	0.890	0.849	0.898	0.884	-
	S4Sleep(ts) ^{f, p}	single	0.817±0.001±0.001	0.931	0.526	0.888	0.848	0.895	0.882	0.977
	S4Sleep(spec) ^{f, p}	single	0.815±0.001±0.0005	0.931	0.505	0.884	0.853	0.931	0.882	0.977
	XSleepNet1 ^{f, p} [15]	multi	0.822	-	-	-	-	-	0.891	-
	XSleepNet2 ^{f, p} [15]	multi	0.823	-	-	-	-	-	0.891	-
	RobustSleepNet ^{g, i} [25]	multi	0.792	-	-	-	-	-	-	-
	U-Sleep ^{h, r} [20]	multi	0.80	0.93	0.51	0.87	0.76	0.92	-	-
	Pei et al 2024 ^{e, m} [22]	multi	0.693	0.938	0.271	0.795	0.641	0.822	0.824	-
S4Sleep(ts) ^{f, p}	multi	0.827±0.001±0.002	0.938	0.536	0.894	0.849	0.919	0.890	0.980	
S4Sleep(spec) ^{f, p}	multi	0.8322±0.0005±0.0001	0.942	0.539	0.898	0.856	0.919	0.895	0.981	

a: based on full SEDF. b: based on SEDF20. c: based on SEDF-SC. d: based on recordings from 20 selected subjects in the full SEDF. e: based on recordings from 100 selected subjects in the SHHS visit 1. f: based on SHHS visit 1. g: based on SHHS visit 2. h: based on full SHHS. i: 3-fold cross-validation. j: 5-fold cross-validation. k: 10-fold cross-validation. l: leave-one-subject-out cross-validation. m: 7:2:1 training-validation-test holdout set evaluation. n: 8:1:1 training-validation-test holdout set evaluation. o: 5:2:3 training-validation-test holdout set evaluation. p: 7:3 training-test holdout set evaluation. q: test on 23 recordings from SEDF-SC. r: test on 140 recordings from full SHHS.

of encoder-predictor models in a structured fashion while also keeping track of the uncertainties of the approach. We envision that this procedure could serve as a blueprint for other long-term time series classification tasks in order to assess if the identified model architectures also generalize to other domains.

Time-series-based vs. spectrogram-based models: The two *S4Sleep* variants show the same ranking on all three considered datasets, namely *S4Sleep(ts)* dominates in the single-channel case and *S4Sleep(spec)* in the multi-channel case. More specifically, on SHHS the differences between both models turn out statistically significant. It remains an interesting open question on how to devise time-series-based models to also outperform spectrogram-based approaches in the multi-channel case. The best-performing approaches in the literature were often the XSleepNet [15] models, which operate jointly on time series and spectrogram input. This suggests that the identified single-modality architectures could be leveraged within a combined model with dual input representations to further enhance the predictive performance.

Single-epoch vs. multi-epoch models: We also use the established methodology to assess the statistical significance of using multiple instead of a single epoch as input. To this end, for given channel configuration and input modality, we compare the best-performing single-epoch model as identified by Table 3 and the best-performing multi-epoch model as identified by Table 4. In all cases, we were able to demonstrate significant performance differences between single- and multi-epoch models at a predefined threshold of 60% of pairwise tests following the methodology introduced above, see also the individual single-epoch results in Table B.8 in the supplementary material. These results reiterate the empirical findings of [16] and emphasize the significant advantage of jointly predicting multiple sleep stages for multiple input epochs at once, which allows to leverage more contextual information into each single-epoch prediction.

Long-range interactions: It is worth pointing out that *S4Sleep(ts)* next to [21] is one of the few approaches that demonstrates the competitiveness of raw time series as sole input representation for sleep staging. In particular, *S4Sleep(ts)* achieved a score that is competitive or even superior to L-SeqSleepNet both on SHHS and SEDF without explicitly leveraging long-range correlations across hundreds of sleep epochs [23], which the authors identify as central aspect for the performance improvement over prior state-of-the-art. A first exploratory study [42] building on the *S4Sleep(ts)*

architecture proposed in this work, showed no performance improvements upon increasing the input size even after gradual upscaling, which puts into question the diagnostic relevance of long range interactions across hundreds of input epochs.

Comparison to literature approaches: The strong results achieved by the proposed methods should be seen as an indication for the use of encoder-predictor models for the purpose of sleep staging and most likely long time series annotation tasks in general. This could also be seen as a hint towards increased architectural simplicity as many of the competing approaches that fall into the encoder-predictor category, see Table 1, rely on custom model components as specific encoder or pooling layers. Apart from the recently proposed S4-layer, which can serve as a drop-in replacement for recurrent or transformer layers, we only leverage standard model components.

Model complexity: Finally, it is worth stressing that all performance comparisons should be set into perspective with the complexity of the underlying model. Even though we acknowledge that the number of model parameters is an imperfect proxy for model complexity, it is most widely reported in the literature. In Table A.6 in the supplementary material, we compare parameter counts of the proposed models to those from models used in the literature. The proposed models reach parameter counts around 5×10^6 and therefore lie in a similar range as competing approaches. Accepting parameter counts as proxy for model complexity, the strong performance of the proposed models is not due to an excessively complex model.

5. Summary and outlook

Summary: In this work, we addressed the problem of automatic sleep staging from polysomnography, which represents a time series classification task where sleep stages have to be predicted per epoch comprising 30 seconds. Based on the specific task, we devise a systematic procedure to identify optimal model architectures for long time series annotation tasks within the search space of encoder-predictor architectures encompassing the majority of literature approaches. During this process, we identify optimal model architectures, $S4Sleep(ts)$ and $S4Sleep(spec)$, for both raw time series and spectrograms as input. Both architectures leverage structured state space models as essential components to extract discriminative representations from the input, albeit in a input-modality specific manner. On full SEDF and SHHS, proposed models outperform all literature approaches in a statistically sig-

nificant manner, both for single-channel as well as multi-channel input. The code underlying our experiments is publicly available [30].

Outlook: We take the fact that both model variants show a very strong performance on SHHS both in the single- and multi-channel input representations without any further hyperparameter adjustments as a sign for the generalization capabilities of the proposed model architectures. We therefore consider it as a very promising step to also explore these models in the context of other data modalities with physiological time series, such as long-term ECG classification, clinical EEG or PPG classification or regression, or even to time series classification task beyond physiological time series such as audio classification or other field. This argument is supported by a recent independent study [43], which identified very similar architectures in the context of robotic sensor data. As briefly discussed in the previous section, there are several directions to further enhance the model performance, ranging from improved architectures for handling multi-channel input to more elaborate pretraining schemes.

Acknowledgment

The authors thank Insa Wolf and Fabian Radtke for discussions.

References

- [1] L. A. Panossian, A. Y. Avidan, Review of sleep disorders, *Medical Clinics of North America* 93 (2) (2009) 407–425.
- [2] M. K. Pavlova, V. Latreille, Sleep disorders, *The American journal of medicine* 132 (3) (2019) 292–299.
- [3] C. Iber, S. Ancoli-Israel, A. L. Chesson, S. F. Quan, et al., *The AASM manual for the scoring of sleep and associated events: rules, terminology and technical specifications*, Vol. 1, American academy of sleep medicine Westchester, IL, 2007.
- [4] J. A. Hobson, A manual of standardized terminology, techniques and scoring system for sleep stages of human subjects, *Electroencephalography and clinical neurophysiology* 26 (6) (1969) 644.
- [5] H. Danker-Hopfe, P. Anderer, J. Zeitlhofer, M. Boeck, H. Dorn, G. Gruber, E. Heller, E. Loretz, D. Moser, S. Parapatics, B. Saletu, A. Schmidt, G. Dorffner, Interrater reliability for sleep scoring according to the Rechtschaffen & Kales and the new AASM standard, *Journal of Sleep Research* 18 (1) (2009) 74–84. doi:10.1111/j.1365-2869.2008.00700.x. URL <https://doi.org/10.1111/j.1365-2869.2008.00700.x>
- [6] R. S. Rosenberg, S. V. Hout, The american academy of sleep medicine inter-scorer reliability program: Sleep stage scoring, *Journal of Clinical Sleep Medicine* 09 (01) (2013) 81–87. doi:10.5664/jcsm.2350. URL <https://doi.org/10.5664/jcsm.2350>
- [7] J. B. Stephansen, A. N. Olesen, M. Olsen, A. Ambati, E. B. Leary, H. E. Moore, O. Carrillo, L. Lin, F. Han, H. Yan, et al., Neural network analysis of sleep stages enables efficient diagnosis of narcolepsy, *Nature communications* 9 (1) (2018) 5229.
- [8] L. Fiorillo, G. Monachino, J. van der Meer, M. Pesce, J. D. Warncke, M. H. Schmidt, C. L. Bassetti, A. Tzovara, P. Favaro, F. D. Faraci, U-sleep’s resilience to aasm guidelines, *NPJ digital medicine* 6 (1) (2023) 33.
- [9] S. Hochreiter, J. Schmidhuber, Long short-term memory, *Neural computation* 9 (8) (1997) 1735–1780.

- [10] A. Vaswani, N. Shazeer, N. Parmar, J. Uszkoreit, L. Jones, A. N. Gomez, L. Kaiser, I. Polosukhin, Attention is all you need, *Advances in neural information processing systems* 30 (2017).
- [11] A. Gu, K. Goel, C. Ré, Efficiently modeling long sequences with structured state spaces, in: *International Conference on Learning Representations*, 2022. [arXiv:2111.00396](https://arxiv.org/abs/2111.00396).
- [12] T. Mehari, N. Strodthoff, Towards quantitative precision for ECG analysis: Leveraging state space models, self-supervision and patient metadata, *IEEE Journal of Biomedical and Health Informatics* (2023) 1–9 [arXiv:2308.15291](https://arxiv.org/abs/2308.15291), [doi:10.1109/jbhi.2023.3310989](https://doi.org/10.1109/jbhi.2023.3310989).
URL <https://doi.org/10.1109/jbhi.2023.3310989>
- [13] W. Zhang, L. Yang, S. Geng, S. Hong, Self-supervised time series representation learning via cross reconstruction transformer, *IEEE Transactions on Neural Networks and Learning Systems* (2024) 1–10 [doi:10.1109/tnnls.2023.3292066](https://doi.org/10.1109/tnnls.2023.3292066).
URL <http://dx.doi.org/10.1109/TNNLS.2023.3292066>
- [14] V. Gorade, A. Singh, D. Mishra, Large scale time-series representation learning via simultaneous low-and high-frequency feature bootstrapping, *IEEE Transactions on Neural Networks and Learning Systems* (2023).
- [15] H. Phan, O. Y. Chén, M. C. Tran, P. Koch, A. Mertins, M. De Vos, Xsleepnet: Multi-view sequential model for automatic sleep staging, *IEEE Transactions on Pattern Analysis and Machine Intelligence* 44 (9) (2021) 5903–5915.
- [16] H. Phan, F. Andreotti, N. Cooray, O. Y. Chén, M. De Vos, Seqsleepnet: end-to-end hierarchical recurrent neural network for sequence-to-sequence automatic sleep staging, *IEEE Transactions on Neural Systems and Rehabilitation Engineering* 27 (3) (2019) 400–410.
- [17] M. M. Bronstein, J. Bruna, T. Cohen, P. Veličković, Geometric deep learning: Grids, groups, graphs, geodesics, and gauges, *arXiv preprint 2104.13478* (2021). [arXiv:2104.13478](https://arxiv.org/abs/2104.13478).
- [18] J. Schmidhuber, Learning complex, extended sequences using the principle of history compression, *Neural Computation* 4 (2) (1992) 234–242.

- [19] Y. LeCun, A path towards autonomous machine intelligence version 0.9. 2, 2022-06-27, Open Review 62 (2022).
- [20] M. Perslev, S. Darkner, L. Kempfner, M. Nikolic, P. J. Jennum, C. Igel, U-sleep: resilient high-frequency sleep staging, *npj Digital Medicine* 4 (1) (Apr. 2021). doi:10.1038/s41746-021-00440-5. URL <https://doi.org/10.1038/s41746-021-00440-5>
- [21] P. An, J. Zhao, B. Du, W. Zhao, T. Zhang, Z. Yuan, Amplitude-time dual-view fused eeg temporal feature learning for automatic sleep staging, *IEEE Transactions on Neural Networks and Learning Systems* (2022).
- [22] W. Pei, Y. Li, P. Wen, F. Yang, X. Ji, An automatic method using mfcc features for sleep stage classification, *Brain Informatics* 11 (1) (2024) 6.
- [23] H. Phan, K. P. Lorenzen, E. Heremans, O. Y. Chén, M. C. Tran, P. Koch, A. Mertins, M. Baumert, K. B. Mikkelsen, M. D. Vos, L-SeqSleepNet: Whole-cycle long sequence modelling for automatic sleep staging, *IEEE Journal of Biomedical and Health Informatics* (2023) 1–10doi:10.1109/jbhi.2023.3303197. URL <https://doi.org/10.1109/jbhi.2023.3303197>
- [24] H. Phan, K. Mikkelsen, O. Y. Chén, P. Koch, A. Mertins, M. De Vos, Sleeptransformer: Automatic sleep staging with interpretability and uncertainty quantification, *IEEE Transactions on Biomedical Engineering* 69 (8) (2022) 2456–2467.
- [25] A. Guillot, V. Thorey, Robustsleepnet: Transfer learning for automated sleep staging at scale, *IEEE Transactions on Neural Systems and Rehabilitation Engineering* 29 (2021) 1441–1451.
- [26] A. Einizade, S. Nasiri, S. H. Sardouie, G. D. Clifford, Productgraph-sleepnet: Sleep staging using product spatio-temporal graph learning with attentive temporal aggregation, *Neural Networks* 164 (2023) 667–680.
- [27] Z. Jin, K. Jia, Sagsleepnet: A deep learning model for sleep staging based on self-attention graph of polysomnography, *Biomedical Signal Processing and Control* 86 (2023) 105062.

- [28] H. Seo, S. Back, S. Lee, D. Park, T. Kim, K. Lee, Intra-and inter-epoch temporal context network (iitnet) using sub-epoch features for automatic sleep scoring on raw single-channel eeg, *Biomedical signal processing and control* 61 (2020) 102037.
- [29] A. Supratak, H. Dong, C. Wu, Y. Guo, Deepsleepnet: A model for automatic sleep stage scoring based on raw single-channel eeg, *IEEE Transactions on Neural Systems and Rehabilitation Engineering* 25 (11) (2017) 1998–2008.
- [30] T. Wang, N. Strodthoff, Source code for: S4Sleep: Elucidating the design space of deep-learning-based long time series classification models—a case study based on sleep staging, github.com <https://github.com/AI4HealthUOL/s4sleep> (Oct. 2023).
- [31] A. Baevski, Y. Zhou, A. Mohamed, M. Auli, wav2vec 2.0: A framework for self-supervised learning of speech representations, *Advances in neural information processing systems* 33 (2020) 12449–12460.
- [32] A. Radford, J. W. Kim, T. Xu, G. Brockman, C. McLeavey, I. Sutskever, Robust speech recognition via large-scale weak supervision, in: *International Conference on Machine Learning*, PMLR, 2023, pp. 28492–28518.
- [33] D.-M. Ross, E. Cretu, Probabilistic modelling of sleep stage and apnoeic events in the university college of dublin database (ucddb), in: *2019 IEEE 10th Annual Information Technology, Electronics and Mobile Communication Conference (IEMCON)*, IEEE, 2019, pp. 0133–0139.
- [34] S. F. Quan, B. V. Howard, C. Iber, J. P. Kiley, F. J. Nieto, G. T. O’Connor, D. M. Rapoport, S. Redline, J. Robbins, J. M. Samet, et al., The sleep heart health study: design, rationale, and methods, *Sleep* 20 (12) (1997) 1077–1085.
- [35] G.-Q. Zhang, L. Cui, R. Mueller, S. Tao, M. Kim, M. Rueschman, S. Mariani, D. Mobley, S. Redline, The national sleep research resource: towards a sleep data commons, *Journal of the American Medical Informatics Association* 25 (10) (2018) 1351–1358.
- [36] B. Kemp, A. H. Zwinderman, B. Tuk, H. A. Kamphuisen, J. J. Obery, Analysis of a sleep-dependent neuronal feedback loop: the slow-wave mi-

- crocontinuity of the eeg, *IEEE Transactions on Biomedical Engineering* 47 (9) (2000) 1185–1194.
- [37] A. L. Goldberger, L. A. Amaral, L. Glass, J. M. Hausdorff, P. C. Ivanov, R. G. Mark, J. E. Mietus, G. B. Moody, C.-K. Peng, H. E. Stanley, Physiobank, physiotoolkit, and physionet: components of a new research resource for complex physiologic signals, *circulation* 101 (23) (2000) e215–e220.
- [38] T.-Y. Lin, P. Goyal, R. Girshick, K. He, P. Dollár, Focal loss for dense object detection, in: *Proceedings of the IEEE international conference on computer vision*, 2017, pp. 2980–2988.
- [39] L. N. Smith, Cyclical learning rates for training neural networks, in: *2017 IEEE winter conference on applications of computer vision (WACV)*, IEEE, 2017, pp. 464–472.
- [40] I. Loshchilov, F. Hutter, Decoupled weight decay regularization, in: *International Conference on Learning Representations*, 2018.
- [41] T. Mehari, N. Strodthoff, Self-supervised representation learning from 12-lead ECG data, *Computers in Biology and Medicine* 141 (2022) 105114. doi:10.1016/j.compbiomed.2021.105114.
URL <https://doi.org/10.1016/j.compbiomed.2021.105114>
- [42] T. Wang, N. Strodthoff, Assessing the importance of long-range correlations for deep-learning-based sleep staging, in: *Workshop Biosignalsm Göttingen, Germany (non-archival)*, 2024. arXiv:2402.17779.
- [43] R. Bhirangi, C. Wang, V. Pattabiraman, C. Majidi, A. Gupta, T. Hellebrekers, L. Pinto, Hierarchical state space models for continuous sequence-to-sequence modeling, arXiv preprint 2402.10211 (2024). arXiv:2402.10211.

Appendix A. Model architectures

Appendix A.1. Single-epoch prediction models

Encoder architectures: For a single-epoch time series input, we utilized an encoder architecture that comprises two one-dimensional convolutional layers. Each layer consists of 128 features, a kernel size of 3, a stride of 2, corresponding to a moderate downsampling factor of 4, interleaved by ReLU activation functions. In the case of spectrogram input, we reshape the input to join frequency and channel dimensions, which subsequently allows to a further processing using one-dimensional convolutions. In this case, we employed a similar encoder structure with two 1D convolutional layers. Here, we use 128 features, a kernel size of 3 and a stride of 1 interleaved by GeLU activation functions. This particular choice was inspired by the encoder used in state-of-the-art speech recognition models operating on spectrograms as input data [32] and reduces to the former in the case of a single input channel. To simplify the notation, we refer to both encoders as *CNN* encoder but refer with it to the respective convolutional encoders for time series/spectrogram data. We also conducted experiments with architectures without explicit encoders (*NONE*), where the input is passed directly to the respective predictor models. In the case of time series input, the input sequence is just processed through a linear layer mapping from the number of input channels to the appropriate model dimension of the predictor model. In the case of spectrogram input, we first reshape channel and frequency axes into a common axis and then proceed with a linear layer as in the case of time series input.

Predictor architectures: We consider three different architectures: A two-layer, bidirectional LSTM model [9], a four-layer transformer model [10], or a four-layer S4 model [11]. To ensure that the total number of trainable parameters and hence the model complexity approximately remains within a same magnitude, we set the model dimensions to 512, 256, and 512 for LSTM, transformers, and S4, respectively. The dropout rates stand at 0.1 for the transformer models and 0.2 for the S4 models. Each transformer layer features 8 heads, while the state dimension of S4 is set to 64. We omitted the transformer predictor coupled with the *NONE* encoder from our evaluation, attributing to the substantially increased computational time associated with this particular configuration.

Prediction head architectures: The prediction head architecture just involves a global average pooling followed by a single linear layer. We refrain

from testing more complex pooling options such as attention-based pooling layer in order to keep the complexity of the search space manageable.

Appendix A.2. Multi-epoch prediction models

For multi-epoch time series input, we consider different strategies.

Encoder architectures: epoch encoders: The first option is to use entire single-epoch models, which have shown superior performance, as encoders. We refer to such encoders as *epoch encoders*. We distinguish different epoch encoders based on the respective encoder-predictor combinations they use. We designate the respective epoch encoders based on their encoder-predictor combinations as *EELSTM* for *CNN+LSTM*, *EETF* for *CNN+TF*, *EES4* for *CNN+S4*, and *EENS4* for *NONE+S4*.

Encoder architectures: strided convolutions for raw time series input: The second option to reach a heavily temporally downsampled intermediate representation that is appropriate for further processing is through the use of strided convolutions. This approach is inspired by encoders used in speech recognition models operating on raw waveform data such as wave2vec [31]. Here, we use four 1D convolutional layers each with feature sizes 512, kernel sizes of 9-9-3-3, and stride sizes of 5-5-2-2, resulting in a temporal downsampling factor of 100, interleaved with ReLU activations. We refer to this encoder as *SCNN* (for strided CNN) encoder.

Encoder architectures: single-epoch encoders for spectrogram input: For multi-epoch spectrogram input, we have the option to utilize the CNN encoder (*CNN*) described in the paragraph on single-epoch encoder. In this case there is no need for a strong temporal downsampling as the spectrograms by themselves already come at a 100 times smaller temporal resolution compared to the original time series input. In this sense, the simple CNN encoder for spectrograms can be regarded as analogue of the strided CNN encoder for raw time series. In addition, we also investigate a second choice from the single-epoch encoder model, namely the *NONE*, i.e., omitting the encoder altogether.

Predictor architectures: The three predictor options are coincide with the predictor architectures described in the single-epoch case in Section Appendix A.1.

Prediction head architectures: The prediction head architecture consists of a single linear layer. Depending on the used encoder choice (i.e., for sub-epoch encoder, *SCNN*, *CNN*, and *NONE* encoders) it is preceded by a local

pooling layer with appropriate kernel size to reduce the temporal resolution of the output to one output token per epoch.

Appendix A.3. Parameter counts

Table A.6 summarizes parameter counts for the proposed models and selected models from the literature.

Model	#parameters
DeepSleepNet [29]	2.30×10^7
SeqSleepNet [16]	1.64×10^6
U-Sleep [20]	3.10×10^6
RobustSleepNet [25]	1.80×10^5
XSleepNet [15]	5.74×10^6
SleepTransformer [24]	3.70×10^6
L-SeqSleepNet [23]	6.30×10^5
<i>S4Sleep(ts)</i>	4.90×10^6
<i>S4Sleep(spec)</i>	5.70×10^6

Table A.6: Parameter counts for the proposed models and models from the literature.

Appendix B. Additional results

Appendix B.1. Epoch encoder vs. sub-epoch encoder

In Table B.7, we investigate the effect of using epoch encoders that operate on fractions of an entire input epoch.

Appendix B.2. Single-epoch models on SEDF

Table B.8 shows the performance of the best-performing single-epoch models from Table 3 trained and evaluated on the SEDF dataset (test set scores). These results provide quantitative insights on the performance gains achieved through predicting several epochs at once.

channels	features	fraction	encoder	predictor	macro F_1
multi	raw	1	EES4	S4	0.820*
		1/2	EES4	S4	0.814*
		1/5	EES4	S4	0.820*
		1/10	EES4	S4	0.814
	spec	1	EENS4	TF	0.815*
		1/2	EENS4	TF	0.818*
		1/5	EENS4	TF	0.800
		1/10	EENS4	TF	0.801
single	raw	1	EES4	S4	0.801*
		1/2	EES4	S4	0.802*
		1/5	EES4	S4	0.804*
		1/10	EES4	S4	0.784
	spec	1	EENS4	TF	0.797*
		1/2	EENS4	TF	0.787
		1/5	EENS4	TF	0.785
		1/10	EENS4	TF	0.785

Table B.7: Comparing epoch encoder and sub-epoch encoder on SEDF based on validation set scores. Notation as in Table 4.

model	channels	macro F_1
CNN+S4(TS)	single	0.752±0.003±0.002
None+S4(Spec)	single	0.730±0.007±0.004
CNN+S4(TS)	multi	0.769±0.002±0.004
None+S4(Spec)	multi	0.780±0.002±0.003

Table B.8: Performance of selected models using a single epoch as input on SEDF. Notation as in Table 4.